Article

Not peer-reviewed version

Aqueous-Phase Formation of Two-Dimensional PbI2 Nanoplates for High-Performance Self-Powered Photodetector

Muhammad Imran Saleem , Perumalveeramalai Chandrasekar , Attia Batool , Jeong-Hwan Lee *

Posted Date: 19 September 2023

doi: 10.20944/preprints202309.1290.v1

Keywords: green-chemistry principles; aqueous-phase synthesis; two-dimensional nanoplates; self-powered photodetector

Article

Aqueous-Phase Formation of Two-Dimensional PbI_2 Nanoplates for High-Performance Self-Powered Photodetector

Muhammad Imran Saleem [1], Perumalveeramalai Chandrasekar [2], Attia Batool [3] and Jeong-Hwan Lee [1,4]*

[1] Department of Materials Science and Engineering, Inha University, Incheon 22212, Republic of Korea
[2] School of Science, Minzu University of China, Beijing, 100081 P.R.China
[3] Research Center for Materials Science, Beijing Institute of Technology, Beijing 100081, P. R. China
[4] 3D Convergence Center, Inha University, Incheon 22212, Republic of Korea
* Correspondence: Jeong-hwan.lee@inha.ac.kr .

Abstract: The research community has shown significant interest in the aqueous synthesis of nanomaterials due to its ability to eliminate the need for complex organic solvents. This synthesis approach aligns with the principles of green chemistry, attracting considerable attention. Aqueous solution technology in fabricating nanostructures has gained recognition for its potential to create ultrasensitive, low-energy, and ultrafast optoelectronic devices. This report focuses on synthesizing lead iodide (PbI_2) nanoplates using a water-based solution technique and fabricating a planar photodetector. The photodetectors with a planar type of device structure (ITO/PbI_2 NPs/Au) demonstrated a remarkable photosensitivity of 3.9×10^3 and a photoresponsivity of 0.51 mA/W at a wavelength of 405 nm. Notably, the asymmetrical output properties of ITO/PbI_2 NPs/Au detector deliver additional evidence of the effective creation of a Schottky contact. Thus, the photodetector exhibited a photoresponse even at 0 V bias, leading to the realization of self-powered photodetectors. Additionally, the device exhibited a rapid photoresponse of 0.21/0.38 s (−5 V) in the visible range. This study has expanded the horizons for the aqueous-phase synthesis of nanoplate nanostructures, enabling the large-area fabrication of high-performance photodetectors.

Keywords: green-chemistry principles; aqueous-phase synthesis; two-dimensional nanoplates; self-powered photodetector

1. Introduction

Over the past few years, various high-performance nanomaterials have been synthesized by solution processes such as hot injection and low-temperature recrystallization techniques [1-3]. While these approaches yield nanomaterials with remarkable photophysical properties, their reliance on highly toxic organic solvents poses significant environmental challenges [4-6]. The RE100 Climate Group, with its primary objective of accelerating the transition to widespread zero carbon grids and its unwavering commitment to achieving 100% renewable electricity, has attracted the participation of renowned electronics companies in recent years. By adopting environmentally friendly techniques, these collaborative efforts aim to ensure a smooth and efficient transition towards widespread zero-carbon grids. For example, global companies plan to enhance their utilization of renewable energy, invest in innovative technologies, and conduct research to create energy-efficient products. The company also aims to augment water reuse practices and explore advancements in carbon capture technology. However, the current method employed to synthesize nanomaterials and device fabrication through various physical and chemical techniques could be more environmentally friendly, adopting RE100 guidelines and green chemistry principles [7,8].

In response, aqueous syntheses of nanomaterials have emerged as an alternative to minimize environmental pollution and implement the guidelines of green chemistry. Moreover, the resulting nanomaterials are dispersed in aqueous media without phase transfer, facilitating their utilization in

 doi:10.20944/preprints202309.1290.v1

biological applications. Among the diverse range of nanomaterials, particular attention has been devoted to layered two-dimensional (2D) materials due to their potential to advance cutting-edge technologies such as electronics, optoelectronics, and sensing applications. Researchers have been actively exploring the unique properties exhibited by 2D materials, particularly in optoelectronics devices [9,10]. Layered 2D materials have found successful applications in optical communication, sensing, and imaging by utilizing ultrabroad wavelength photodetectors. Significantly, the remarkable feature of layered 2D materials lies in their flexibility and adaptability to different materials and substrates, making them highly advantageous. Surprisingly, these materials exhibit a unique characteristic of being free from dangling bonds, which typically contribute to surface recombination and an increase in the dark current [11-13].

Despite the remarkable properties of 2D materials, the fabrication of 2D material structures has succeeded by stacking exfoliated 2D flakes or 2D thin films grown via chemical vapor deposition (CVD), utilizing a layer-by-layer transfer technique. However, this transfer method faces significant challenges, such as potential interface contamination, limited scalability, and a lack of precise control over the stack configuration. Thus, the production of 2D materials-based optoelectronic devices on a large scale is of utmost importance and relies heavily on advancements in processing techniques for advanced materials. There is a strong desire to develop a solution-processed approach, as this method holds great promise for constructing novel optoelectronic devices with outstanding performance.

Here, PbI_2 nanoplates (NPs) with diverse morphologies, including hexagonal nanoplates, truncated triangular nanoplates, and tri-pyramidal nanoplates, were synthesized using an aqueous solution of PbI_2. The solution process involved simply dropping the solution onto a pre-cleaned ITO substrate that had been preheated to 90 °C to form thin films, enabling the achieve large-area fabrication as well. The optoelectronic properties of PbI_2 NPs were assessed by fabricating planar photodetector ITO/PbI_2 NP/Au device structure, which exhibited a high photosensitivity of 3.9×10^3 and a photoresponsivity of 0.51 mA/W (−2V) at a wavelength of 405 nm. Moreover, the device demonstrated a rapid photoresponse with a speed of 0.21/0.38 s within the visible range.

2. Materials and Methods

All the chemical reagents were of analytical grade and used as received without further purification. Lead (II) iodide (PbI_2, 99.9985%) was purchased from Alfa Aesar.

2.1. Synthesis of 2D PbI_2 Nanoplates

First, PbI_2 (4 mg/mL) was mixed in 3 mL DI water and magnetically stirred at 90°C for 30 min. The solution becomes clear with negligible sedimentation. Then, 30-40μL of clear supernatant solution was dropped onto a glass substrate prior to heating at 90°C for 10-15 min.

2.2. Device Fabrication

Pre-patterned indium tin oxide (ITO) glass substrates were each cleaned with acetone, isopropyl alcohol, and then deionized water for 15 minutes in an ultrasonic bath. Furthermore, substrates have been treated with UV ozone to make the surface hydrophilic. Then, as mentioned above, 2D PbI_2 nanosheets were grown by the drop-casting method. Finally, all devices were completed by thermally evaporating a 100 nm Au electrode. A thermal evaporator is located at the 3D Convergence Center of Inha University. The active area of the device is 4 mm^2, defined by the intersection of ITO and Au stripes.

2.3. Characterizations

The XRD pattern of samples was characterized by Rigaku Ultima IV X-ray diffractometer using Cu Kα radiation (λ=1.5406 Å). Scanning electron microscopy (SEM) images were acquired by ZEISS sigma 500 field emission SEM operated at an accelerating voltage of up to 30 kV. The optical UV-absorption spectra were measured with a spectrometer (Perkin Elmer, Lambda 750). The current-voltage (*I-V*) characteristics of the devices were measured using a Keithley 4200 SCS unit. A 405 nm

Preprints (www.preprints.org) | NOT PEER-REVIEWED | Posted: 19 September 2023 doi:10.20944/preprints202309.1290.v1

laser diode was used as the light source for the photocurrent measurement, while the power of the incident radiation was tuned and measured with a power meter.

3. Results

The PbI_2 nanosheets were synthesized by a low-temperature solution processing method, as shown schematically in **Figure 1a-b**. The crystal structure of PbI_2 is analogous to other transition metal dichalcogenides (such as MoS_2, S-Mo-S), indicating that a layer of lead (Pb) atoms are covalently linked to two layers of iodide (I) atoms, forming the repeated hexagonal structure [14,15]. The interaction between adjacent layers with a spacing of 6.78 Å is governed by a weak van der Waals force, as indicated in **Figure 1c-d.**

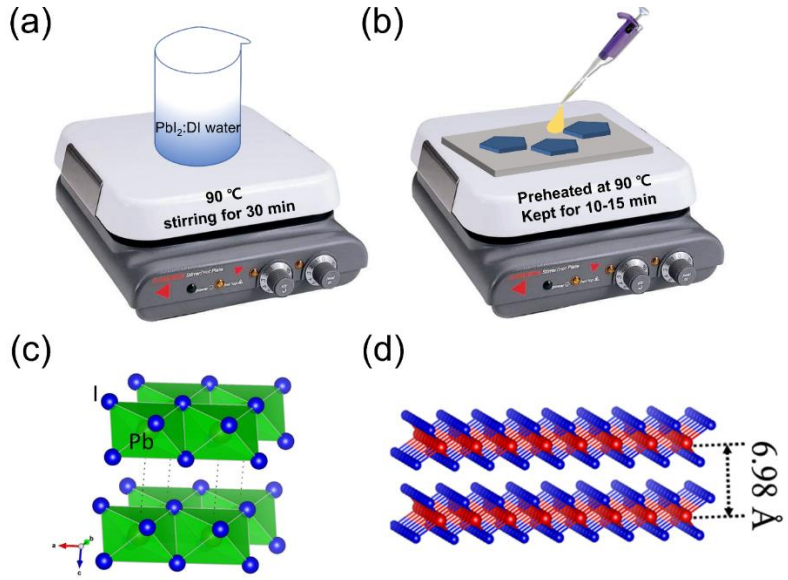

Figure 1. The schematic illustration of 2D PbI_2 precursor preparation and 2D PbI_2 nanoplates deposition on a glass substrate. **(c)** Single unit cell of PbI_2. **(d)** Layered PbI_2 crystal structure separated with a distance of 6.98 Å.

The shape of the as-synthesized PbI_2 nanoplates was visualized by optical microscopy (OM). The OM confirmed the orientation distribution of triangular, pyramidal, and hexagonal PbI_2 nanosheets synthesized by a simple solution method (**Figure 2a-c**). Furthermore, the uniformity and controllability of the thickness in three morphologies of the as-prepared PbI_2 layered crystal are further confirmed by scanning electron microscopy (SEM), as shown in **Figure 2d-h**. The literal size and thickness of the single crystal of PbI_2 are estimated from OM and SEM, and the values are about 20 μm and 550–600 nm, respectively (**Figure 2a-h**). The results confirmed that the solution-processed method effectively fabricates the uniform shapes of 2D PbI_2 layered crystals. The nucleation probability of PbI_2 is determined by $A_1 \propto \exp[-1/\alpha^2]$, where A_1 is the nucleation rate of crystals, and α is the supersaturation degree. The change in morphology of the PbI_2 crystal is derived from the difference in each crystal's growth rate. As predicted by theoretical calculation, the low-index plane (001) of PbI_2 has the lowest surface energy value [16,17]. The least surface energy value (0.48 J/m^2) and low-index plane are favorable for nucleation probability. The growth rate of PbI_2 nanoplates along the low-index (001) plane in the literal direction (*a*- and *b*-axis) is much higher than in the vertical direction (*c*-axis), resulting in the formation of the nanoplates with larger width-to-thickness ratio.

The crystal structure of as-grown two-dimensional PbI_2 nanoplates was characterized by X-ray diffraction (XRD). The 2D PbI_2 NPs have four sharp and distinct diffraction peaks located at 12.24°, 25°, 38.19° and 52.02°, which can be assigned to (001), (002), (003) and (004) crystal planes of hexagonal PbI_2 (JCPDS, No.73-1750, space group: P-3m1) [18]. These peaks indicate lamellar stacking along the

Preprints (www.preprints.org) | NOT PEER-REVIEWED | Posted: 19 September 2023 doi:10.20944/preprints202309.1290.v1

c-axis of the I-Pb-I sandwich layer (**Figure 3a**) [19]. The optical properties of PbI_2 NPs have been analyzed, and the UV-visible absorption spectrum is shown in **Figure 3b**. One can clearly observe the absorption peaks centered at 498 nm. The optical bandgap was estimated by Tauc plot, corresponding to 2.36 eV (**Figure 3c**). The calculated bandgap is in good agreement with previous reports [20,21]. These results confirm the structural and optical quality of as-synthesized 2D PbI_2 nanoplates, which are urgently needed for the fabrication of high-performance optoelectronic devices.

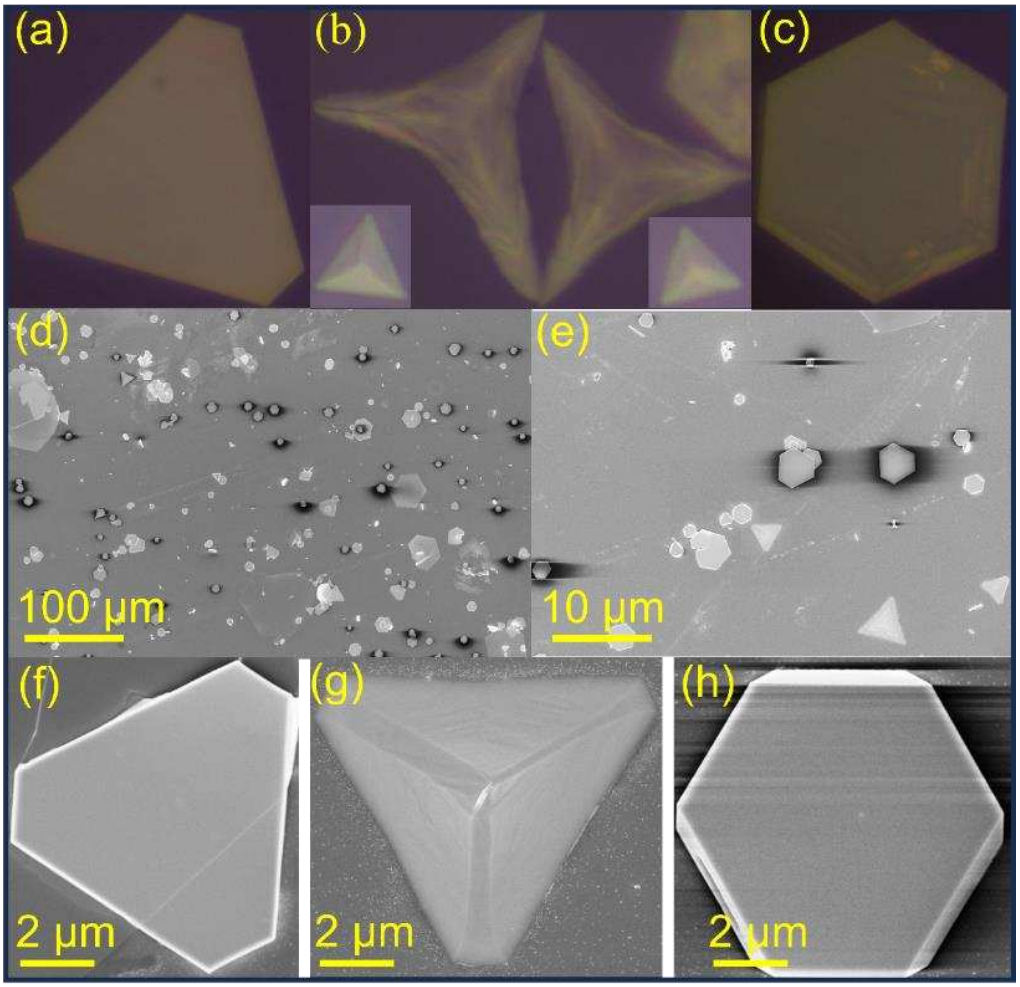

Figure 2. (a-c) Optical Microscopic image of PbI_2 nanoplates with different morphologies. **(d- e)** SEM images of PbI_2 nanoplates. **(f-h)** SEM image of PbI_2 nanoplates with different structural morphology.

The facile solution-processed method has been employed for well-defined 2D PbI_2 nanoplates that are suitable for optoelectronic applications. As a state-of-the-art application, a photodetector with ITO (150 nm)/PbI_2/Au (100 nm) configuration was adopted to evaluate the optoelectronic properties of 2D PbI_2 nanoplates. In comparison, the Au top electrode (100 nm) was thermally evaporated (schematically illustrated in **Figure 4a**). The corresponding energy levels diagram of the photodetector is shown in **Figure 4b**; all the fundamental values were taken from previous literature [20,22,23]. The light response of the photodetector was studied under the 405 nm light illumination with different power densities (0.1, 0.3, 0.5, and 1.5 mW/cm^2). The extremely low value of dark current ~0.9 pA and photocurrent of 6.5×10^{-8} A at −2 V with an impressive photocurrent/dark current ratio of 10^4 can be witnessed from current *vs* voltage (*I-V*) curves, which is good for high-performance narrow-band photodetectors (**Figure 4c**) [16]. We have further extended our analysis by increasing the power density (0.1, 0.3, 0.5, 1.5 mW/cm^2). The results show the increase in photocurrent with increasing the power of 405 nm illumination that the efficiency of the photogenerated charge carriers is proportional to the number of photon flux absorbed.

Preprints (www.preprints.org) | NOT PEER-REVIEWED | Posted: 19 September 2023 doi:10.20944/preprints202309.1290.v1

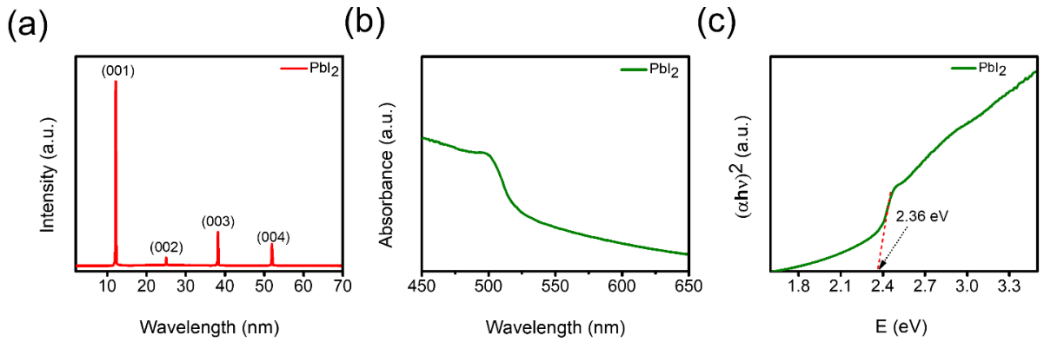

Figure 3. (a) XRD pattern of PbI_2 nanoplates. **(b)**The UV-Vis absorption spectrum of PbI_2 nanoplates. **(c)** Tauc plot of as-grown two-dimensional PbI_2 nanoplates.

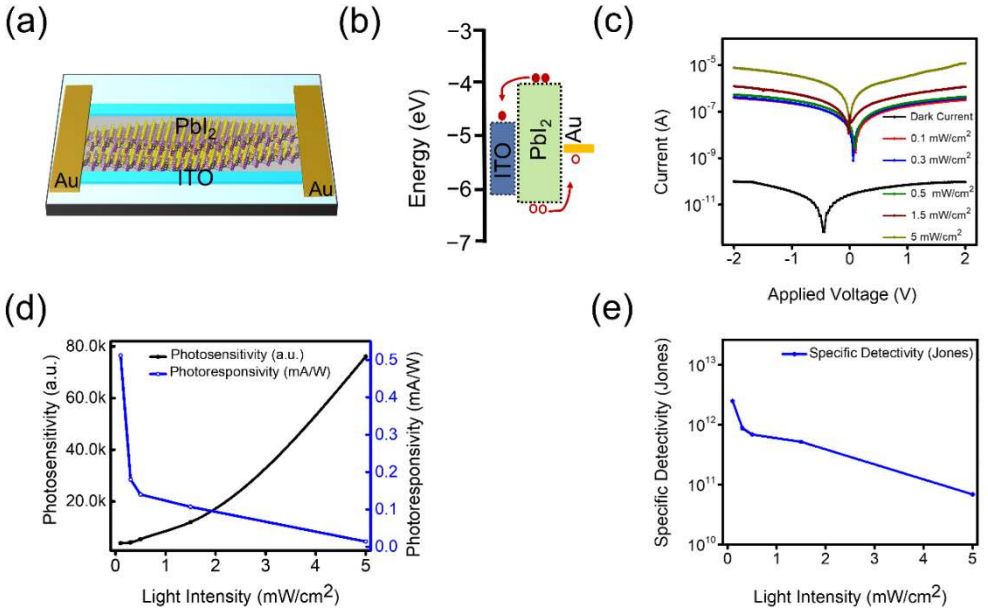

Figure 4. (a) Schematic illustration of PbI_2 nanoplate photodetector. **(b)** The band diagram illustrates the charge transport mechanism of the photodetector at zero bias. **(c)** The current-voltage curve of a photodetector in the dark and under the illumination of light with different intensity. **(d)** Photosensitivity and photoresponsivity as a function of light intensity. **(e)** Specific detectivity (D^*) as a function of light intensity.

Under the UV-light illumination with a peak of 405 nm, the electron-hole pairs were generated, and electrons were injected into the ITO side. At the same time, holes were collected through the Au electrode. Notably, the photodetector configuration used here is free of carrier transport layers, which would affect the operational stability of fabricated devices. Consequently, the better stability of our device is expected. The rectifying characteristics are responsible for conferring the self-powered photodetector capability (**Figure 4c**), and this phenomenon can be attributed to the creation of Schottky junctions between the metal electrodes and the p-type PbI_2 nanoplates. At an applied voltage of 0 V, the photocurrent exhibits a notable upward shift, providing further evidence of the self-powered nature of the device [22,24,25]. This phenomenon results from the energy differential between the anode and cathode, resulting in a built-in potential of approximately 0.11 V.

The analytical calculation was performed to evaluate photodetector performance, and photosensitivity (K) is the ability to distinguish an incident light from a dark condition [26,27]. It can be quantified as $K = \frac{I_{ill} - I_{dark}}{I_{dark}}$, where I_{ill} and I_{dark} are photocurrent and dark current, and K=3.9×10³ is achieved under 0.1 mW/cm² 405 nm illumination. The photosensitivity K as a function of the power density is plotted in **Figure 4d**, showing an increasing trend with increasing power density. In addition, key parameters such as photoresponsivity (R) and specific detectivity (D^*) are well-suited

Preprints (www.preprints.org) | NOT PEER-REVIEWED | Posted: 19 September 2023 doi:10.20944/preprints202309.1290.v1

to assess photodetector performance, which can be defined as $R = \frac{I_{ph}}{P_{ill}}$, where P_{ill} is attributed to the power density. The maximum photoresponsivity is 0.51 mA/W at −2 V under 0.1 mW/cm² 405 nm. The specific detectivity (D^*), which is the ability to minimum impinging optical power that a detector can distinguish from noise signal and can be expressed as follows, $D^* = R\sqrt{\frac{S}{2qI_{dark}}}$, where q is the elementary charge, R is photoresponsivity and S is the active area. The specific detectivity D^* is calculated to be 2.5 ×10¹² Jones at −2 V and is even better than previously reported (see **Table 1**). The R and D^* as a function of power densities are plotted in **Figure 4 d, e**. From here we can see that R and D^* decrease as a function of increasing power density owing to the compound loss in the device. All key values are comparable to CVD/PVD grown PbI_2 NPs (**see Table 1**).

The photocurrent response illustrates the durability of optoelectronic devices for practical applications. The transient photoresponse of our photodetector was measured by periodically switching the 5 mW/cm² 405 nm light at −5 V at a constant interval for several cycles (**Figure 5a**). When the light is turned-on, the photocurrent is generated, and the photocurrent quickly decays while the light is turned off, as shown in Figure 5a. The highly stable and repeatable photo-switching performance of the 2D PbI_2 NPs photodetector can be attributed to the fact that the photoresponse remains almost unchanged even after 250 seconds of continuous operation. The rise and decay times of photodetector are the times taken for the photocurrent to increase from 10% to 90% of the peak value and *vice versa [24,25,28].* As plotted in Figure 5b-c, the rise and decay time of our device is 0.21/0.38 s. Therefore, the results were believed to have provided a deep insight into the efficient application of PbI_2 nanosheets for high-performance optoelectronic devices.

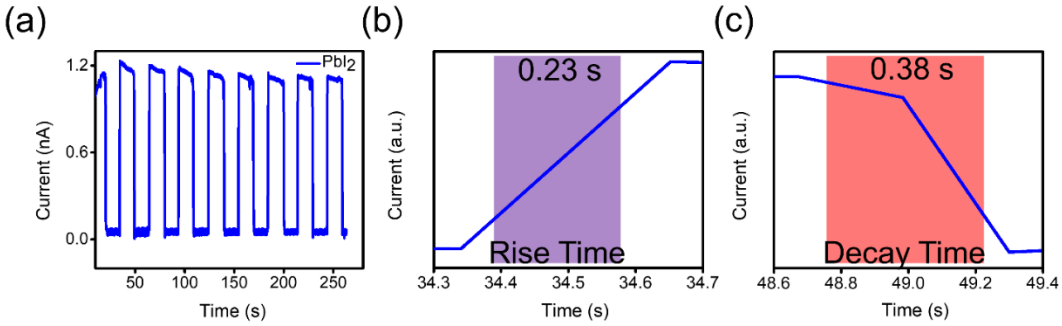

Figure 5. (a) Temporal response of PbI_2 photodetector. **(b)** Rising time and **(c)** decay time.

Table 1. Comparison of various key properties of different representative PbI_2-Based Photodetectors

Device Configuration	Growth Mechanism	Light Intensity	Photosensitivity (*K*)	Responsivity (*R*)	Detectivity D^* (Jones)	Rise/Fall Time (sec)	Ref.
ITO/PbI_2/Au	Solution-process	0.1 mW/cm²	3.9×10³	0.5 mA/W	2.5×10¹²	0.21/0.38 s	This Work
ITO/PbI_2/Ni	Solution-process	1.14 mW/mm²	-	0.65 A/W	0.95×10¹³	2/3 ms	[20]
SiO_2/Si/PbI_2/Au	PVD-grown†	40 mW/cm²	-	-	-	18/22 ms	[16]
PET/Graphene/PbI_2	PVD-grown	5 μW/cm²	-	45 A/W	-	35/20 μs	[14]

/ Graphene							
SiO_2/Si/SbSI/PbI_2/Ag	Hydrothermal method	0.1 mW/cm^2	-	26.3 mA/W	-	12/8 ms	[29]
Ti/Au/PbI_2/Au	Solution-process	0.17 mW/cm^2	-	40 mA/W	3.31×10^{10}	161.7/192 ms	[17]
Si/PbI_2-$MAPbI_2$/Ti/Au	PVD-grown	-	-	410 mA/V	3.1×10^{11}	1.4/0.9 s	[30]
Au/PbI_2/Au	PVD-grown	3.4 mW/cm^2	-	147.6 40 A/W	2.56×10^{12}	18/25 ms	[19]
SiO_2/Si/WS_2/PbI_2/Au	PVD-grown	0.01 mW/cm^2	-	7.1×10^4 A/W	-	26.4/28.9 ms	[31]
Polyimide/PbI_2/Au	Hydrothermal method	-	-	5 mA/W	-	30 ms	[32]
Si/SiO_2/PbI_2/Au	PVD-process	-	-	13 mA/W	-	425/41 ms	[33]

†PVD-physical vapor deposition

4. Conclusions

In summary, we have fabricated solution-processed photodetectors based on 2D PbI_2 nanoplates. The structural and optical properties of as-synthesized PbI_2 nanoplates have been carefully analyzed. The nucleation and growth mechanism of PbI_2 nanoplates is briefly explained based on structural properties. The PbI_2 nanosheets thus synthesized were used to fabricate PDs with the asymmetric electrode configuration ITO/PbI_2/Au. The PD showed a light response at 0 V bias under 405 nm light illumination with a light intensity of 0.1 mW/cm^2, which is attributed to the variation in the work function of the electrodes, as explained. The high photoresponsivity and specific detectivity of 0.51 mA/W and 2.5×10^{12} Jones at −2 V, respectively were achieved with our device configuration (ITO/PbI_2 NPs/Au). In addition, the device has shown a quick response of 0.23 s and a decay of 0.38 s at −5 V under illumination of 5 mW/cm^2 visible light. Given the results presented here with PbI_2 nanoplates and their promising application to photodetectors, future advances in processing and fabrication techniques are anticipated.

Author Contributions: M. I. Saleem: Conceptualization, investigation, data analysis, and writing—original draft preparation. Perumalveeramalai Chandrasekar: Data analysis. A. Batool: Optical Properties analysis. J.-H. Lee: writing—review and editing, supervision, funding acquisition. All authors have read and agreed to the published version of the manuscript.

Funding: This research was supported by Basic Science Research Program through the National Research Foundation of Korea (NRF) funded by the Ministry of Education (No.2022R1A6A1A03051705). This research was also supported by the Inha University Research Grant.

Data Availability Statement: All the relevant data are given in this paper.

Conflicts of Interest: There is no conflict of interest.

References

1. Proppe, A. H.; Berkinsky, D. B.; Zhu, H.; Šverko, T.; Kaplan, A.E.K.; Horowitz, J.R.; Kim, T.; Chung, H.; Jun, S.; Bawendi, M.G. Highly stable and pure single-photon emission with 250 ps optical coherence times in InP colloidal quantum dots. *Nat. Nanotechn.* **2023**, doi:10.1038/s41565-023-01432-0.
2. Septianto, R. D.; Miranti, R.; Kikitsu, T.; Hikima, T.; Hashizume, D.; Matsushita, N.; Iwasa, Y.; Bisri, S. Z. Enabling metallic behaviour in two-dimensional superlattice of semiconductor colloidal quantum dots. *Nat. Commun.* **2023**, *14*, 2670, doi:10.1038/s41467-023-38216-y.
3. Ahn, N.; Livache, C.; Pinchetti, V.; Jung, H.; Jin, H.; Hahm, D.; Park, Y.-S.; Klimov, V. I. Electrically driven amplified spontaneous emission from colloidal quantum dots. *Nature* **2023**, *617*, 79-85, doi:10.1038/s41586-023-05855-6.
4. Chen, X.; Lin, X.; Zhou, L.; Sun, X.; Li, R.; Chen, M.; Yang, Y.; Hou, W.; Wu, L.; Cao, W.; et al. Blue light-emitting diodes based on colloidal quantum dots with reduced surface-bulk coupling. *Nat. Commun.* **2023**, *14*, 284, doi:10.1038/s41467-023-35954-x.
5. Protesescu, L.; Yakunin, S.; Bodnarchuk, M. I.; Krieg, F.; Caputo, R.; Hendon, C. H.; Yang, R. X.; Walsh, A.; Kovalenko, M. V. Nanocrystals of Cesium Lead Halide Perovskites ($CsPbX_3$, X = Cl, Br, and I): Novel Optoelectronic Materials Showing Bright Emission with Wide Color Gamut. *Nano Lett.* **2015**, *15*, 3692-3696, doi:10.1021/nl5048779.
6. Lee, J. W.; Kim, D. Y.; Baek, S.; Yu, H.; So, F. Inorganic UV–Visible–SWIR Broadband Photodetector Based on Monodisperse PbS Nanocrystals. *Small* **2016**, *12*, 1328-1333, doi:https://doi.org/10.1002/smll.201503244.
7. Singh, D. K.; Verma, D. K.; Singh, Y.; Hasan, S. H. Preparation of CuO nanoparticles using Tamarindus indica pulp extract for removal of As(III): Optimization of adsorption process by ANN-GA. *J. Environ. Chem. Eng.* **2017**, *5*, 1302-1318, doi:https://doi.org/10.1016/j.jece.2017.01.046.
8. Nassar, N. N.; Husein, M. M. Effect of microemulsion variables on copper oxide nanoparticle uptake by AOT microemulsions. *J. Colloid Interf. Sci.* **2007**, *316*, 442-450, doi:https://doi.org/10.1016/j.jcis.2007.08.044.
9. Cheng, Z.; Zhao, T.; Zeng, H. 2D Material-Based Photodetectors for Infrared Imaging. *Small Sci.* **2022**, *2*, 2100051, doi:https://doi.org/10.1002/smsc.202100051.
10. Liu, C.; Guo, J.; Yu, L.; Li, J.; Zhang, M.; Li, H.; Shi, Y.; Dai, D. Silicon/2D-material photodetectors: from near-infrared to mid-infrared. *Light: Sci. & Appl.* **2021**, *10*, 123, doi:10.1038/s41377-021-00551-4.
11. Long, M.; Wang, P.; Fang, H.; Hu, W. Progress, Challenges, and Opportunities for 2D Material Based Photodetectors. *Adv. Funct. Mater.* **2019**, *29*, 1803807, doi:https://doi.org/10.1002/adfm.201803807.
12. Ezhilmaran, B.; Patra, A.; Benny, S.; M. R, S.; V. V, A.; Bhat, S. V.; Rout, C. S. Recent developments in the photodetector applications of Schottky diodes based on 2D materials. *J. Mater. Chem. C* **2021**, *9*, 6122-6150, doi:10.1039/D1TC00949D.
13. Li, F.; Zheng, J.; Yao, Q.; Bie, Y.-Q. Recent progress of silicon integrated light emitters and photodetectors for optical communication based on two-dimensional materials. *Opt. Mater. Exp.* **2021**, *11*, 3298-3320, doi:10.1364/OME.435902.
14. Zhang, J.; Huang, Y.; Tan, Z.; Li, T.; Zhang, Y.; Jia, K.; Lin, L.; Sun, L.; Chen, X.; Li, Z.; et al. Low-Temperature Heteroepitaxy of 2D PbI_2/Graphene for Large-Area Flexible Photodetectors. *Adv. Mater.* **2018**, *30*, 1803194, doi:https://doi.org/10.1002/adma.201803194.
15. Sun, Y.; Zhou, Z.; Huang, Z.; Wu, J.; Zhou, L.; Cheng, Y.; Liu, J.; Zhu, C.; Yu, M.; Yu, P.; et al. Band Structure Engineering of Interfacial Semiconductors Based on Atomically Thin Lead Iodide Crystals. *Adv. Mater.* **2019**, *31*, 1806562, doi:https://doi.org/10.1002/adma.201806562.
16. Zhong, M.; Zhang, S.; Huang, L.; You, J.; Wei, Z.; Liu, X.; Li, J. Large-scale 2D PbI_2 monolayers: experimental realization and their indirect band-gap related properties. *Nanoscale* **2017**, *9*, 3736-3741, doi:10.1039/C6NR07924E.
17. Wang, R.; Li, S.; Wang, P.; Xiu, J.; Wei, G.; Sun, M.; Li, Z.; Liu, Y.; Zhong, M. PbI_2 Nanosheets for Photodetectors via the Facile Cooling Thermal Supersaturation Solution Method. *J. Phys. Chem. C* **2019**, *123*, 9609-9616, doi:10.1021/acs.jpcc.9b01322.
18. Wang, Y.; Gan, L.; Chen, J.; Yang, R.; Zhai, T. Achieving highly uniform two-dimensional PbI_2 flakes for photodetectors via space confined physical vapor deposition. *Science Bull.* **2017**, *62*, 1654-1662, doi:https://doi.org/10.1016/j.scib.2017.11.011.
19. Zhong, M.; Huang, L.; Deng, H.-X.; Wang, X.; Li, B.; Wei, Z.; Li, J. Flexible photodetectors based on phase dependent PbI_2 single crystals. *J. Mater. Chem. C* **2016**, *4*, 6492-6499, doi:10.1039/C6TC00918B.
20. Liu, D.; Chen, R.; Liu, F.; Zhang, J.; Zhuang, X.; Yin, Y.; Wang, M.; Sa, Z.; Wang, P.; Sun, L.; et al. Flexible Omnidirectional Self-Powered Photodetectors Enabled by Solution-Processed Two-Dimensional Layered PbI_2 Nanoplates. *ACS Appl. Mater. Interf.* **2022**, *14*, 46748-46755, doi:10.1021/acsami.2c13373.
21. Li, C.; Li, W.; Cheng, M.; Yang, W.; Tan, Q.; Wang, Q.; Liu, Y. High Sensitive and Broadband Photodetectors Based on Hybrid PbI_2 Nanosheet/CdSe Nanobelt. *Adv. Opt. Mater.* **2021**, *9*, 2100927, doi:https://doi.org/10.1002/adom.202100927.
22. Saleem, M. I.; Yang, S.; Zhi, R.; Li, H.; Sulaman, M.; Chandrasekar, P. V.; Zhang, Z.; Batool, A.; Zou, B. Self-powered, all-solution processed, trilayer heterojunction perovskite-based photodetectors. *Nanotechn.* **2020**, *31*, 254001, doi:10.1088/1361-6528/ab7de7.

23. Saleem, M. I.; Yang, S.; Zhi, R.; Sulaman, M.; Chandrasekar, P.V.; Jiang, Y.; Tang, Y.; Batool, A.; Zou, B. Surface Engineering of All-Inorganic Perovskite Quantum Dots with Quasi Core–Shell Technique for High-Performance Photodetectors. *Adv. Mater. Interf.* **2020**, *7*, 2000360, doi:https://doi.org/10.1002/admi.202000360.
24. Sulaman, M.; Yang, S.; Bukhtiar, A.; Tang, P.; Zhang, Z.; Song, Y.; Imran, A.; Jiang, Y.; Cui, Y.; Tang, L.; et al. Hybrid Bulk-Heterojunction of Colloidal Quantum Dots and Mixed-Halide Perovskite Nanocrystals for High-Performance Self-Powered Broadband Photodetectors. *Adv. Funct. Mater.* **2022**, *32*, 2201527, doi:https://doi.org/10.1002/adfm.202201527.
25. Saleem, M. I.; Yang, S.; Batool, A.; Sulaman, M.; Veeramalai, C.P.; Jiang, Y.; Tang, Y.; Cui, Y.; Tang, L.; Zou, B. $CsPbI_3$ nanorods as the interfacial layer for high-performance, all-solution-processed self-powered photodetectors. *J. Mater. Sci. & Techn.* **2021**, *75*, 196-204, doi:https://doi.org/10.1016/j.jmst.2020.07.049.
26. Saleem, M. I.; Sulaman, M.; Batool, A.; Bukhtiar, A.; Khalid, S. Suppression of Mid-Gap Trap State in $CsPbBr_3$ Nanocrystals with Br-Passivation for Self-Powered Photodetector. *Energy Techn.* **2023**, 2300013, doi:https://doi.org/10.1002/ente.202300013.
27. Sulaman, M.; Song, Y.; Yang, S.; Saleem, M. I.; Li, M.; Perumal Veeramalai, C.; Zhi, R.; Jiang, Y.; Cui, Y.; Hao, Q.; et al. Interlayer of PMMA Doped with Au Nanoparticles for High-Performance Tandem Photodetectors: A Solution to Suppress Dark Current and Maintain High Photocurrent. *ACS Appl. Mater. & Interf.* **2020**, *12*, 26153-26160, doi:10.1021/acsami.0c04093.
28. Sulaman, M.; Yang, S.; Imran, A.; Zhang, Z.; Bukhtiar, A.; Ge, Z.; Song, Y.; Sun, F.; Jiang, Y.; Tang, L.; et al. Two Bulk-Heterojunctions Made of Blended Hybrid Nanocomposites for High-Performance Broadband, Self-Driven Photodetectors. *ACS Appl. Mater. & Interf.* **2023**, *15*, 25671-25683, doi:10.1021/acsami.3c01749.
29. Sun, L.; Wang, C.; Xu, L.; Wang, J.; Liu, X.; Chen, X.; Yi, G.-C. SbSI whisker/PbI_2 flake mixed-dimensional van der Waals heterostructure for photodetection. *CrystEngComm* **2019**, *21*, 3779-3787, doi:10.1039/C9CE00544G.
30. Lan, C.; Dong, R.; Zhou, Z.; Shu, L.; Li, D.; Yip, S.; Ho, J.C. Large-Scale Synthesis of Freestanding Layer-Structured PbI_2 and $MAPbI_3$ Nanosheets for High-Performance Photodetection. *Adv. Mater.* **2017**, *29*, 1702759, doi:https://doi.org/10.1002/adma.201702759.
31. Qi, Z.; Yang, T.; Li, D.; Li, H.; Wang, X.; Zhang, X.; Li, F.; Zheng, W.; Fan, P.; Zhuang, X.; et al. High-responsivity two-dimensional p-PbI_2/n-WS_2 vertical heterostructure photodetectors enhanced by photogating effect. *Mater. Horiz.* **2019**, *6*, 1474-1480, doi:10.1039/C9MH00335E.
32. Sun, L.; Wang, C.; Xu, L.; Wang, J.; Chen, X.; Yi, G.-C. Millimeter-sized PbI_2 flakes and $Pb_5S_2I_6$ nanowires for flexible photodetectors. *J. Mater. Chem. C* **2018**, *6*, 7188-7194, doi:10.1039/C8TC01657G.
33. Han, M.; Sun, J.; Bian, L.; Wang, Z.; Zhang, L.; Yin, Y.; Gao, Z.; Li, F.; Xin, Q.; He, L.; et al. Two-step vapor deposition of self-catalyzed large-size PbI_2 nanobelts for high-performance photodetectors. *J. Mater. Chem. C* **2018**, *6*, 5746-5753, doi:10.1039/C8TC01180J.